Heat Capacity and Phonon Dispersion in Poly(L-Methionine)

POONAM TANDON,[1] V. D. GUPTA,[2] O. PRASAD,[1] SHANTANU RASTOGI,[1] V. P. GUPTA[1]

[1] Physics Department, Lucknow University, Lucknow 226 007, India

[2] Division of Biopolymers, Central Drug Research Institute, Lucknow 226 001, India

Received 24 October 1996; revised 7 April 1997; accepted 23 April 1997

ABSTRACT: Poly(L-methionine) (PMet) is one of the two sulfur containing polyamino acids. Raman, FTIR spectra, and heat capacity measurements of PMet have been well interpreted through the normal mode analysis and the density of states derived therefrom. Earlier interpretation of heat capacity data is limited because it is based on the Tarasov model, wherein the concept of group frequency and skeletal similarity are used. A special feature of some dispersion curves is their tendency to bunch in the neighborhood of the helix angle. This has been attributed to the presence of strong intramolecular interactions. Repulsion between the dispersion curves is also observed.
 J Polym Sci B: Polym Phys **35:** 2281–2292, 1997
Keywords: conformation; phonon dispersion; α-helix; normal modes; poly(L-leucine); density of states; heat capacity

INTRODUCTION

In continuation of our recent publication in this journal on left-handed α poly(β benzyl-L-aspartate), we report here similar studies on poly(L-methionine) (PMet), one of the two sulfur-containing polyamino acids that is found to exist preferably in a right-handed α-helical conformation in solid state.[1] Unlike the case of poly(L-serine) and poly(*S*-methyl-L-cysteine) where a hetro atom is present at the β carbon, poly(L-methionine) has it at the γ position. This facilitates the formation of β-sheet structure in the former and α-helix in the latter.[2] The presence of α-helix in PMet is also supported by ORD measurement.[3] Fasman et al. have reported that the α-helix of PMet is less stable than that of poly(L-leucine) and poly(L-alanine).[2] However, it has greater stability than poly(γ-benzyl-L-glutamate) and poly(β-benzyl-L-aspartate), which have polar side chains.

In some recent publications Wunderlich and Bu,[4] Bu et al.,[5] Roles and Wunderlich,[6] and Roles et al.[7] have reported theoretical as well as experimental studies on heat capacities of a variety of polymeric systems, synthetic as well as biopolymeric. In most of the cases their analysis is based on the separation of the vibrational spectrum into group and skeletal vibrations. The former are taken from computations fitted to IR and Raman data, and the latter by using the two parameter Tarasov model and fitting to the low-temperature heat capacities. However, in a few cases, where detailed dispersion curves of the vibrational spectra are available, they have been used for obtaining group and skeletal vibrations and number of vibrators of each type. In some cases dispersion curves for one polymeric system have been used to obtain the number of vibrators and frequencies of box oscillators for polymers with an identical backbone. This approach is alright when full dispersion curves are not available. However, it has its own limitations, especially when the side-chain and backbone modes are strongly coupled.

Vibrational spectroscopy plays an important role in the elucidation of polymer structures. Normal mode analysis helps in precise assignment and identification of spectral features. Thus, the information contained in the complex IR/Raman spectrum is better understood. The art of finger

Correspondence to: V. D. Gupta

Journal of Polymer Science: Part B: Polymer Physics, Vol. 35, 2281–2292 (1997)
 CCC 0887-6266/97/142281-12

printing cannot succeed here. Recently, Gani et al. have reported F. T. Raman studies for PMet.[8] In continuation of our ongoing work, we present here a study of the normal modes and their dispersion and heat capacity data for PMet. This group has previously carried out vibrational analysis and phonon dispersion for a variety of biopolymers having α, ω, 3_{10} helical, and β-sheet conformation.[9–18] The heat capacity is in very good agreement with the experimental data of Roles et al.[7]

THEORY AND EXPERIMENT

Calculation of Normal Modes

The calculation of normal mode frequencies has been carried out according to Wilson's G.F. Matrix method[19] as modified by Higgs[20] for an infinite chain using Urey Bradley–Shimanouchi force field, which takes into account nonbonded interactions. The Wilson *GF* matrix method consists of writing the inverse kinetic energy matrix G and the potential energy matrix F in internal coordinates R. In the case of infinite isolated helical polymer, there is an infinite number of internal coordinates that leads to G and F matrices of infinite order. Due to the screw symmetry of the polymer, a transformation similar to that given by Born and Von Karman can be performed, which reduces the infinite problem to finite dimensions. The transformation consists of defining a set of symmetry coordinates

$$S(\delta) = \sum_{s=-\infty}^{\infty} R^n \exp(is\delta) \tag{1}$$

where δ is the vibrational phase difference between the corresponding modes of the adjacent residue units.

The elements of the $G(\delta)$ and $F(\delta)$ matrices have the form:

$$G_{ik}(\delta) = \sum_{s=-\infty}^{\infty} G_{ik}^{s} \exp(is\delta) \tag{2}$$

$$F_{ik}(\delta) = \sum_{s=-\infty}^{\infty} F_{ik}^{s} \exp(is\delta) \tag{3}$$

The vibrational secular equation, which gives normal mode frequencies and their dispersion as a function of phase angles, has the form:

$$|G(\delta)F(\delta) - \lambda(\delta)I| = \theta, \quad 0 \le \delta \le \pi \tag{4}$$

The vibration frequencies $\nu(\delta)$ (in cm^{-1}) are related to eigen values $\lambda(\delta)$ by the following relation:

$$\lambda(\delta) = 4\pi^2 c^2 \nu^2(\delta) \tag{5}$$

For any given phase difference δ (other than 0 or π), the $G(\delta)$ and $F(\delta)$ matrices are complex. To avoid the difficulties involved in handling complex numbers, methods have been devised to transform the complex matrices into equivalent real matrices by constructing suitable linear combinations of coordinates. One method of transforming a complex matrix to its real matrix equivalent is through a similarity transformation. It can be shown that any complex matrix $H = M + iN$ can be replaced by the real ones:

$$\begin{vmatrix} M & -N \\ N & M \end{vmatrix}$$

In the present case, we can write $G(\delta) = G^R(\delta) + iG^I(\delta)$ and $F(\delta) = F^R(\delta) + iF^I(\delta)$, where $G^R(\delta), F^R(\delta), G^I(\delta), F^I(\delta)$ are the real and imaginary parts of $G(\delta)$ and $F(\delta)$. The product $H(\delta) = G(\delta)F(\delta)$ becomes

$$H(\delta) = \begin{vmatrix} G^R(\delta) & -G^I(\delta) \\ G^I(\delta) & G^R(\delta) \end{vmatrix} \times \begin{vmatrix} F^R(\delta) & -F^I(\delta) \\ F^I(\delta) & F^R(\delta) \end{vmatrix}$$

$$= \begin{vmatrix} H^R(\delta) & -H^I(\delta) \\ H^I(\delta) & H^R(\delta) \end{vmatrix} \tag{6}$$

where

$$H^R(\delta) = G^R(\delta)F^R(\delta) - G^I(\delta)F^I(\delta) \tag{7}$$

$$H^I(\delta) = G^R(\delta)F^I(\delta) + G^I(\delta)F^R(\delta) \tag{8}$$

The matrix $H(\delta)$ now has dimensions $2N \times 2N$. The eigen values, therefore, occur in pairs of equal values. The difficulty of dealing with complex numbers is thus avoided.

In the present work, the Urey Bradley force field has been used, which takes into account both bonded and nonbonded interactions as well as internal torsions. The potential energy can be written as

$$V = \sum_{m,j,k} K'_{jk} r_{jk}^{(m)} (\Delta r_{jk}^{(m)}) + K_{jk} (\Delta r_{jk}^{(m)})^2/2 + \sum_{m,i,j,k} H'_{ijk} r_{ij}^{(m)} r_{jk}^{(m)} (\Delta\alpha_{ijk}^{(m)})$$

$$+ H_{ijk} r_{ij}^{(m)} r_{jk}^{(m)} (\Delta\alpha_{ijk}^{(m)})^2/2 + \sum_{m,i,j,k} F'_{ik} q_{ik}^{(m)} (\Delta q_{ik}^{(m)}) + F_{ik} (\Delta q_{ik}^{(m)})^2/2 + \sum_j K_j^{\tau} (\Delta\tau_j)^2 + \sum_j K_j^{\omega} (\Delta\omega_j)^2 \quad (9)$$

where the symbols have their usual meaning. The primed quantities are introduced as internal tensions. Nonbonded interactions involve attraction and repulsion of atoms due to the overlap of their electron shells. These effects are usually expressed by the 6-exp or 6–12 type potentials.

Calculation of Heat Capacity

One of the important uses of dispersion curves is that the microscopic behavior of a crystal can be correlated with its macroscopic properties such as heat capacity. For a one-dimensional system the density-of-states function or the frequency distribution function, which expresses the way energy is distributed among the various branches of normal modes in the crystal, is calculated from the relation

$$g(\nu) = \sum_j (\partial\nu_j/\partial\delta)^{-1} | \nu_j(\delta) = \nu \quad (10)$$

The sum is over all branches j. Considering a solid as an assembly of harmonic oscillators, the frequency distribution $g(\nu)$ is equivalent to a partition function. It can be used to compute thermodynamic quantities such as free energy, entropy, heat capacity, and enthalpy. The constant volume heat capacity is obtained using the following relation, which is based on Born, Von Karman, and Debye's approach

$$C_v = \sum_j g(\nu_j) k N_A (h\nu_j/kT)^2 \times \frac{\exp(h\nu_j/kT)}{[\exp(h\nu_j/kT) - 1]^2} \quad (11)$$

with

$$\int g(\nu_j) d\nu_j = 1$$

The constant volume heat capacity C_v, given by eq. (11) is converted into constant pressure heat capacity C_p using the Nernst–Lindemann approximation[4]

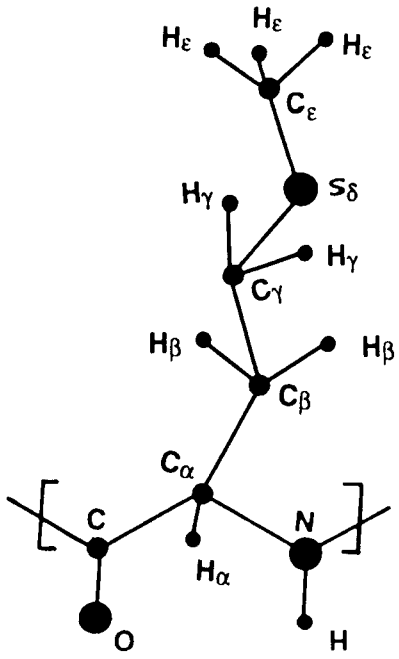

Figure 1. Chemical repeat unit of poly(L-methionine).

$$C_p - C_v = 3RA_o(C_p^2 T/C_v T_m^{\circ}) \quad (12)$$

where A_o is a constant often of a universal value [3.9×10^{-3} (K mol)/J] and T_m° is the estimated equilibrium melting temperature, which is taken to be 573 K.[7] Equation (12) has been tested for several biopolymers with side groups ranging from hydrogen in polyglycine to —CH_2—C_6H_4—OH in poly(L-tyrosine).

The PMet (Lot No. 124F50331, DP(vis)91, Mw(vis)12,000) was purchased from the Sigma Chemicals, St. Louis, MO. The FTIR spectra (4000–150 cm^{-1}), recorded in CSI on a Perkin–Elmer 1800 spectrophotometer, is shown in Figure 2. Before running the spectra the equipment was well purged with dry nitrogen.

RESULTS AND DISCUSSION

In PMet there are 17 atoms per residue, giving rise to 51 dispersion curves (Fig.1). The vibrational frequencies were calculated for different δ values in the interval of 0 to π in step of 0.05 π. The modes corresponding to $\delta = 0, \psi, 2\psi$ are optically active, where ψ is the angle of rotation that separates the adjacent units about the helix axis. For PMet, the value of ψ is $5\pi/9$. All the modes above 1400 cm^{-1} except amide I and II are nondispersive. Hence, only modes below this are shown

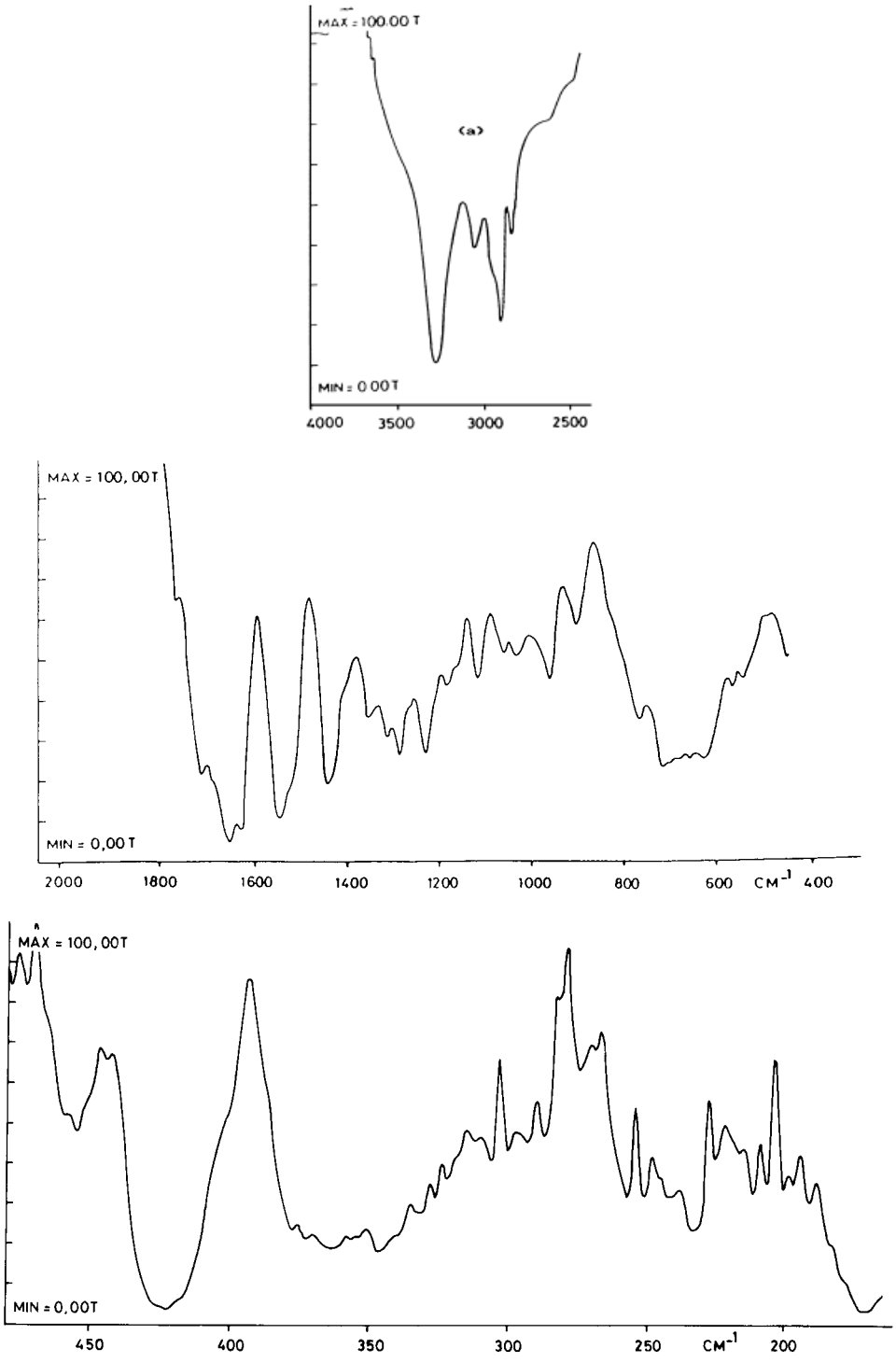

Figure 2. (a) FTIR spectra of α poly(L-methionine) (4000–2500 cm^{-1}). (b) FTIR spectra of α poly(L-methionine) (2000–400 cm^{-1}). (c) FTIR spectra of α poly(L-methionine) (475–150 cm^{-1}).

in Figures 3(a), 4(a), and 5(a). Initially, the force constants for an α-helical backbone have been taken from the helical poly(L-alanine) and for side-chain methylene from poly(L-phenylalanine).[9,13] Then they were modified to give a best fit to the experimental data. The final set of force constants are given in Table I. The assignments of normal-mode frequencies are done on the basis

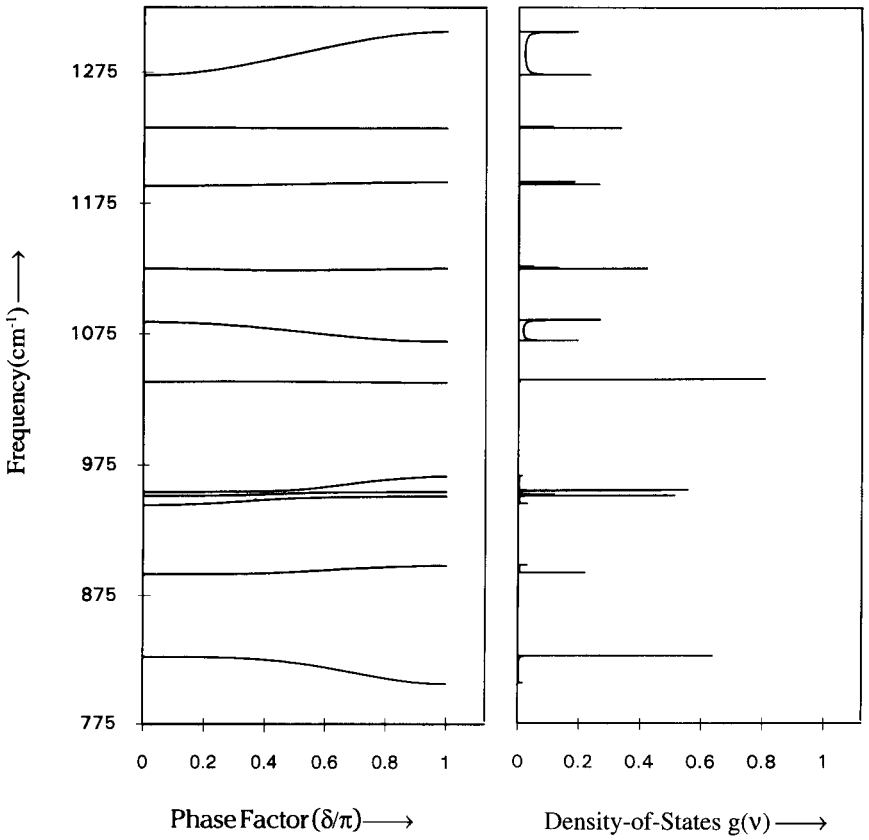

Figure 3. (a) Dispersion curves of poly(L-methionone) (1300–775 cm^{-1}). (b) Density of states $g(\nu)$ (1300–775 cm^{-1}).

of potential energy distributions (P.E.D.), line intensity/profile, second derivative spectra, and the presence/absence of the modes in the molecules having atoms placed in similar environment. The calculated and observed frequencies of dispersive and nondispersive modes along with their assignments are given in Tables II and III, respectively. The two lowest lying branches ($\delta = 0$ and $\delta = 5\pi/9$, $\nu = 0$) are four acoustic modes that correspond to the rotation about helix axis and translations parallel and perpendicular to the helix axis. For the sake of simplicity, the modes are discussed under two separate sections viz. backbone and side-chain modes.

Backbone Modes

Modes involving the motion of main-chain atoms

$$(-\mathrm{C}(-)-\mathrm{C}_\alpha(-)-\mathrm{N}(-)-)$$

are termed as backbone modes. These modes are marked with asterisk in Tables II and III. Amide groups of polypeptides are strong chromophores in IR absorption, and these groups give rise to strong characteristic bands (Amide A, I to VII). The correlation among these characteristic bands and conformations have been found to be useful for conformational diagnosis of polypeptides. A comparison of the amide modes of various polypeptides having an α-helical conformation, is given in Table IV.

Amide A band arising due to N—H stretch vibration is characteristic of its functional group. This mode is highly sensitive to the strength of (N—H$\cdots$O==C) H-bonding. Our calculated Amide A frequency at 3299 cm^{-1} is assigned to the observed one at 3296 cm^{-1}, which is somewhat higher than N—H stretch in 3_{10} helical polypeptides (around 3260 cm^{-1}), reflecting a weaker H-bonding and stronger N—H bonding. This is further supported by the fact that (N$\cdots$O) distance in case of 3_{10} helix is 2.83 Å but in case of α-helical polypeptides this distance is 2.93 Å to 3 Å.[22]

The vibrational modes giving rise to amide I and II bands consist principally of the C==O stretching, N—H in-plane bending and C==N

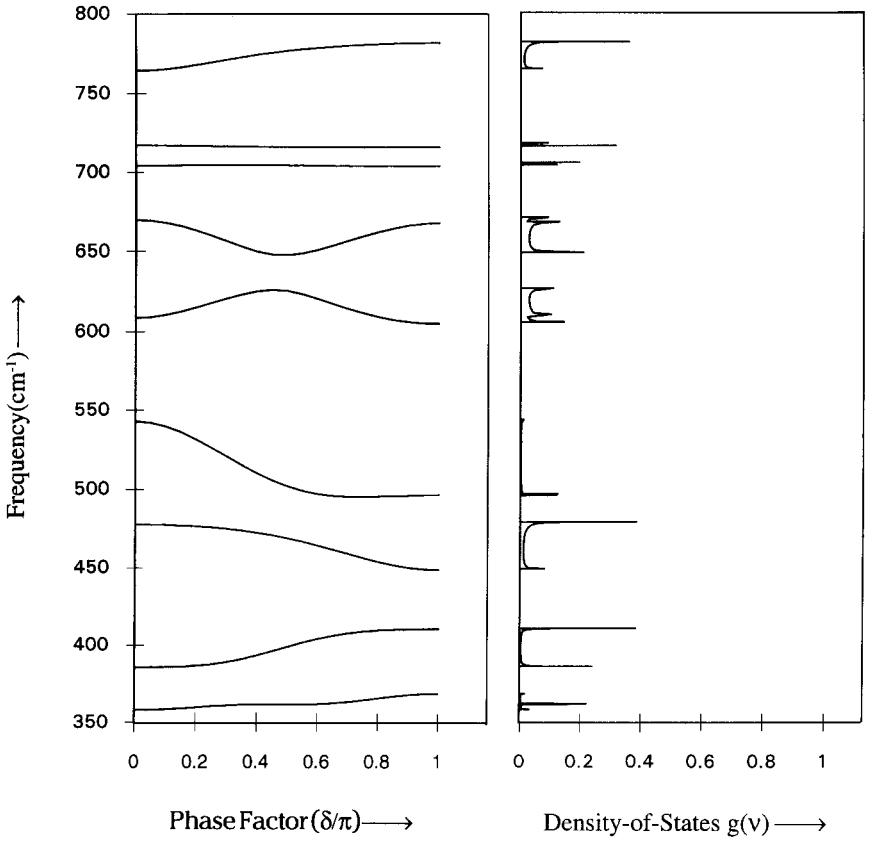

Figure 4. (a) Dispersion curves of poly(L-methionine) (800–350 cm^{-1}). (b) Density of states $g(\nu)$ (800–350 cm^{-1}).

stretching modes of the amide group. These modes are localized in the amide group and as such are not very sensitive to the chain conformation. The amide I calculated at 1651 cm^{-1} is assigned to 1656 cm^{-1}. The amide II is calculated at 1540 cm^{-1} corresponding to the observed peak at 1546 cm^{-1}.

In our calculations, amide III is at 1273 cm^{-1}, corresponding to the observed peak at 1288 cm^{-1} and shows a dispersion of 33 cm^{-1}. For amide III mode, the contribution of N—Cα stretch increases and those of C==N and C==O stretches decreases as δ values are progressed.

The amide V and VI consist of out-of-plane bending vibrations of N—H and C==O respectively, which are asymmetric with respect to CONH plane. Owing to the large component of N—H out-of-plane bending in amide V mode, it is very sensitive to the strength of hydrogen bonding. A mode calculated at 670 cm^{-1} (observed at 656 cm^{-1}) is a mixture of amide V and amide VI. With increase in δ the contribution of ω(C==O) increases up to $\delta = \psi$ and starts decreasing thereafter. The contribution of ω(N—H) to P.E.D. shows a completely reverse trend. C==O in plane bending also mixes with this mode and has increasing contribution to P.E.D. with δ. At the zone boundary this mode becomes a mixture of amide V(22%) and amide IV(24%).

A low-frequency mode appearing at 906 cm^{-1} in FTIR and calculated at 891 cm^{-1} is characteristic of an α-helix and shows sensitivity to the chain conformation. Such a characteristic peak has also been observed at 907 cm^{-1} in α poly(L-alanine).[9]

The amide VII arising due to torsional motion about C==N bond is a better characteristic of conformations. This mode is calculated at 257 cm^{-1} corresponding to the observed one at the same frequency. At $\delta = 0$, this mode largely consists of τ(C==N), τ(Cα—C), and τ(N—Cα). In addition to this, because of the helical conformation, a certain amount of mixing of ϕ(Cα—C==N) has also taken place. Similar mixing have also been reported in the case of an α form of poly(L-alanine),[9] poly(α-aminoisobutyric acid),[18] but not in case of a β-form of poly(L-alanine).[10] The frequency of amide VII decreases with the increase in δ values, as in case of α PLA and PAIB (3_{10} helix).

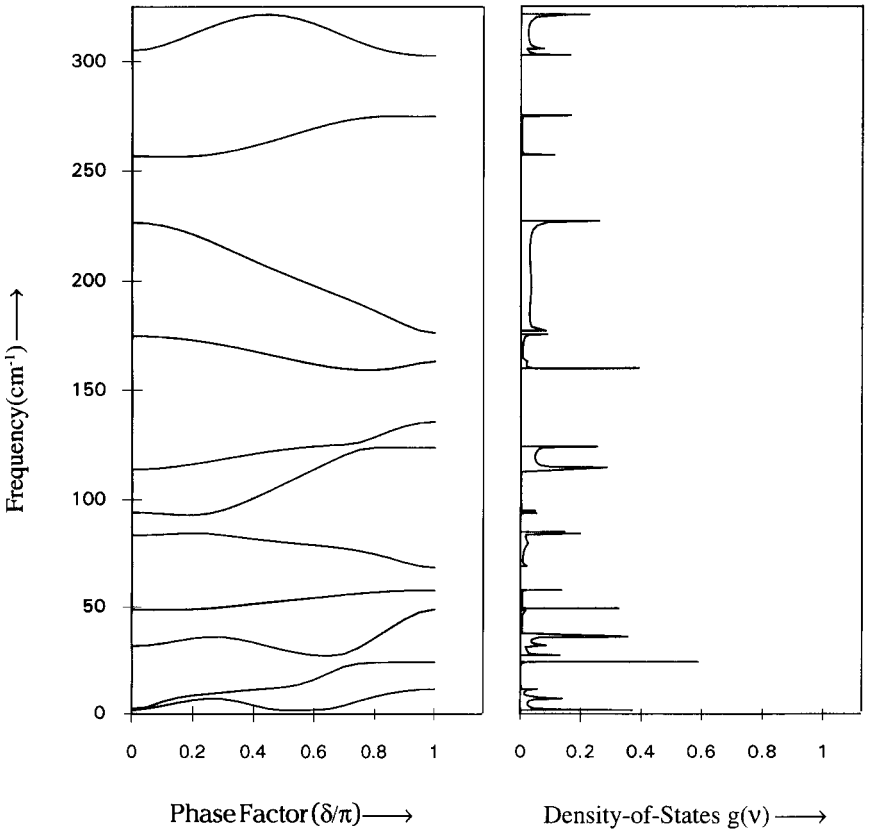

Figure 5. (a) Dispersion curves of poly(L-methionine) below 350 cm^{-1}. (b) Density of states $g(\nu)$ below 350 cm^{-1}.

Amide IV to VII do not appear as pure backbone modes. The P.E.D. in these modes have contributions from the side chain. The frequencies of these modes also do not depend solely on the main-chain conformation, but side-chain structure in question plays an important role, as shown by a comparitive study of amide modes (Table IV).

For a pair of modes calculated at 828 and 764 cm^{-1} (observed at 838 and 766 cm^{-1}, respectively), the contribution of ω(C==O) and ω(N—H), in the former first increases and then starts decreasing slightly as δ/π values approach unity. Reverse behavior is observed in case of the latter mode at 764 cm^{-1}.

The dispersion curves provide information on the extent and degree of coupling. Two interesting features that are observed in dispersion curves are: (a) tendency of some curves to crowd or close in near $\delta = \psi$, which is indicative of coupling between various modes, and (b) repulsion between some dispersion curves. The phenomenon of crowding has been observed in two pairs of modes, (670, 609 cm^{-1}) and (114, 94 cm^{-1}). The first is a mixture of ω(N—H) and ω(C==O). The second consists mainly of bending modes around the Cα atom. This characteristic feature has been noticed in polytraflurothylene (15/7)[23] and α-PLA (18/5),[9] and has been attributed in both cases to strong intramolecular interactions stabilizing the helical structure.

As an example of repulsion, the modes having 94 cm^{-1} and 114 cm^{-1} frequencies at $\delta = 0$, come close together around $\delta = 0.70\pi$ and then repel, with the latter mode taking up nearly constant frequency thereafter. These modes have the same symmetry.[24] Such repulsions have been recently observed in some ω helical polypeptides.[13,14]

On deuteration, the frequency shift calculated was in the general range observed in several other α-helical polypeptides.[22]

Side-Chain Modes

The side chain of PMet consists of two methylene groups at the β and γ positions, a sulphur atom at the δ position, and terminates with a methyl group. The calculated methyl bendings both asymmetric and symmetric at 1476 and 1401 cm^{-1} have been assigned to the observed frequencies at 1475 and 1401 cm^{-1}, respectively. The calculated

Table I. Internal Coordinates and Force Constants (md/Å)

ν(Cα—N)	2.800	ϕ(Cα—Cβ—H$\beta\beta$)	0.445 (0.25)
ν(Cα—Cβ)	3.450	ϕ(H$\beta\beta$—Cβ—Cγ)	0.432 (0.25)
ν(Cβ—H$\beta\alpha$)	4.081	ϕ(Cγ—Sδ—Cε)	0.230 (0.33)
ν(Cβ—Cγ)	3.850	ϕ(Cβ—Cγ—H$\gamma\alpha$)	0.464 (0.25)
ν(Cγ—H$\gamma\alpha$)	4.190	ϕ(H$\gamma\beta$—Cγ—H$\gamma\alpha$)	0.385 (0.27)
ν(Cγ—Sδ)	2.370	ϕ(Sδ—Cε—H$\varepsilon\beta$)	0.425 (0.25)
ν(Sδ—Cε)	2.450	ϕ(Sδ—Cε—H$\varepsilon\gamma$)	0.425 (0.25)
ν(Cε—H$\varepsilon\alpha$)	4.310	ϕ(H$\varepsilon\alpha$—Cε—H$\varepsilon\beta$)	0.419 (0.26)
ν(Cα—C)	2.500	ϕ(H$\varepsilon\beta$—Cε—H$\varepsilon\gamma$)	0.419 (0.26)
ν(C==O)	8.200	ϕ(H$\varepsilon\alpha$—Cε—H$\varepsilon\gamma$)	0.419 (0.26)
ν(C==N)	5.750	ϕ(Sδ—Cε—H$\varepsilon\alpha$)	0.425 (0.25)
ν(N—H)	5.330	ϕ(C==N—H)	0.327 (0.65)
ν(Cα—H)	4.040	ϕ(C==N—Cα)	0.780 (0.35)
ν(Cβ—H$\beta\beta$)	4.081	ϕ(H—N—Cα)	0.310 (0.60)
ν(Cγ—H$\gamma\beta$)	4.190	ϕ(Cα—C==O)	0.300 (0.60)
ν(Cε—H$\varepsilon\beta$)	4.310	ϕ(Cα—C==N)	0.200 (0.60)
ν(Cε—H$\varepsilon\gamma$)	4.310	ϕ(O==C==N)	0.610 (0.90)
		ϕ(Cβ—Cγ—Sδ)	0.420 (0.60)
ϕ(N—Cα—H)	0.2750 (0.80)		
ϕ(N—Cα—C)	0.240 (0.50)	ω(C==O)	0.600
ϕ(H—Cα—C)	0.420 (0.50)	ω(N—H)	0.140
ϕ(N—Cα—Cβ)	0.350 (0.50)		
ϕ(H—Cα—Cβ)	0.355 (0.50)	τ(Cα—C)	0.025
ϕ(C—Cα—Cβ)	0.520 (0.18)	τ(C==N)	0.032
ϕ(Cα—Cβ—H$\beta\alpha$)	0.445 (0.25)	τ(Cα—Cβ)	0.035
ϕ(H$\beta\beta$—Cβ—H$\beta\alpha$)	0.373 (0.22)	τ(Cβ—Cγ)	0.020
ϕ(H$\beta\alpha$—Cβ—Cγ)	0.432 (0.25)	τ(Cγ—Sδ)	0.030
ϕ(Cα—Cβ—Cγ)	0.850 (0.22)	τ(Sδ—Cε)	0.040
ϕ(H$\gamma\alpha$—Cγ—Sδ)	0.480 (0.24)	τ(Cα—N)	0.025
ϕ(H$\gamma\alpha$—Cγ—Sδ)	0.480 (0.24)		

ν, ϕ, ω, τ denote stretch, angle bend, wag, and torsion, respectively. Nonbonded force constants are given in parentheses.

CβH$_2$ and CγH$_2$ scissoring modes at 1442 and 1427 cm^{-1} are assigned to the observed peaks at 1442 and 1425 cm^{-1}, respectively. In the modes calculated at 1392 and 1348 cm^{-1} (observed at 1382 and 1356 cm^{-1}, respectively) there is considerable mixing of CβH$_2$ wag with the side chain (C—C) stretchings and bending of the Hα atom. The CγH$_2$ wag is calculated at 1367 cm^{-1} and assigned to the observed peak at 1356 cm^{-1}.

The modes calculated at 944 and 891 cm^{-1} corresponding to the observed peaks at 962 and 905 cm^{-1} involve the motion of backbone as well as side-chain atoms. The former mode is a mixture of CβH$_2$ rock and skeletal stretching vibrations, whereas the P.E.D. of latter mode shows a mixing of CβH$_2$ rock with skeletal stretchings and skeletal bendings. The CγH$_2$ rock is assigned to the observed peak at 838 cm^{-1}. In the case of poly(L-glutamic acid) the modes involving scissoring, wagging, twisting, and rocking motions of CβH$_2$ and CγH$_2$ groups also fall in the same region.

The characteristic modes identified with sulphur atom are calculated at 712 and 704 cm^{-1} and observed at 718 and 697 cm^{-1}, respectively. They are mainly comprised of a S—Cε stretch for the former case and a S—Cγ stretch for the latter mode. These assignments are consistent with those given by Gani et al.[8]

Heat Capacity

Recently, heat capacity measurements for a series of polyamino acids were reported by Roles et al.[7] and fitted according to Tarasov's two-parameter model. This approach basically involves separation of vibrational spectra into group and skeletal spectra and obtaining the number of vibrators for each case. These are obtained from the dispersion curves and spectra of polymers having the same skeletal structure [e.g., polyglycine II and α poly(L-alanine) for PMet]. This is a crude approximation because even if the skeletal topology

Table II. Nondispersive Modes

Cal.	Obs.	Assignments {% P.E.D. at δ=O}	
3299	3296*	ν(N—H)(100)	
2973	2980*	ν(Cα—Hα)(99)	
2968	2960	CεH$_3$ d-stretch	
2916	2918	CεH$_3$ s-stretch	
2916	2918	CεH$_3$ s-stretch	
2905	2916	CγH$_2$ a-stretch	
2877	2880	CβH$_2$ a-stretch	
2866	2852	CγH$_2$ s-stretch	
2834	2852	CβH$_2$ s-stretch	
1651	1656*	ν(C==O)(59)+ν(C==N)(22)	{Amide I}
1540	1546*	ϕ(H—N—Cα)(34)+ϕ(C==N—H)(31)+ν(C==N)(22)	{Amide II}
1476	1475	CεH$_3$ d-deform	
1476	1475	CεH$_3$ d-deform	
1448	1442	CβH$_2$ scis(30)+ CγH$_2$ scis(43)+ ν(Cβ—Cγ)(15)	
1427	1425	CβH$_2$ scis(50)+CγH$_2$ scis(38)	
1401	1401	CεH$_3$ s-deform	
1392	1382	CγH$_2$ wag(18)+CβH$_2$ wag(13)+ϕ(Hα—Cα—C)(16)+ ν(Cα—Cβ)(11)+ν(Cβ—Cγ)(10)+ϕ(Hα—Cα—Cβ)(8)	
1367	1356	CγH$_2$ wag(66)+ϕ(Hα—Cα—C)(8)	
1348	1356	CβH$_2$ wag(26)+ϕ(Hα—Cα—C)(20)+ϕ(N—Cα—Hα)(14)+ ν(Cα—Cβ)(9)+ν(Cβ—Cγ)(6)+ν(C==O)(5)	
1319	1316	ϕ(N—Cα—Hα)(44)+ϕ(Hα—Cα—Cβ)(37)	
1232	1232	CγH$_2$ twist(86)	
1188	1188	CβH$_2$ twist(86)+ν(Cα—N)(9)	
1125	1118	ν(Cα—N)(33)+ν(Cα—Cβ)(24)+ν(Cα—C)(8)+ϕ(C—Cα—Cβ)(5)	
1039	1034	ν(Cβ—Cγ)(57)	
954	962	CεH$_3$ rock	
951	962	CεH$_3$ rock	
944	962*	ν(Cα—C)(17)+CβH$_2$ rock(26)+CεH$_3$ rock(9)+ ν(C==N)(7)+ν(C==O)(6)	
891	906	CβH$_2$ rock(27)+ϕ(C==N—Cα)(8)+ϕ(O==C==N)(8)+ ν(Cα—N)(7)+CγH$_2$ rock(6)+ν(C==O)(6)+ν(Cα=C)(6)	
717	712	ν(Sδ—Cε)(93)	
704	697	ν(Cγ—Sδ)(72)+ϕ(Cβ—Cγ—Sδ)(8)	
358	363	τ(Cγ—Sδ)(15)+ϕ(Cγ—Sδ—Cε)(15)+ϕ(Cα—C==O)(13) + τ(Cβ—Cγ)(13)+ϕ(O==C==N)(9)+ϕ(Cα—Cβ—Cγ)(8)+τ(Cα—Cβ)(7)	
94	—	τ(Cγ—Sδ)(24)+ϕ(N—Cα—Cβ)(10)+ϕ(Cβ—Cγ—Sδ)(9)+ τ(Cα—Cβ)(9)+ϕ(Cγ—Sδ—Cε)(8)+ϕ(C==N—Cα)(7)+ϕ(Cα—C==N)(6)	
84	—	τ(N—Cα)(14)+ϕ(N—Cα—C)(13)+τ(Cγ—Sδ)(12)+ ϕ(Cα—Cβ—Cγ)(11)+ϕ(N—Cα—Cβ)(11)+τ(Cα—C)(9)+τ(C==N)(8)	
49	—	τ(Cβ—Cγ)(66)+τ(Cα—Cβ)(7)	
32	—	τ(Cα—Cβ)(42)+ϕ(Cα—C==N)(11)+ϕ(N—Cα—Cβ)(8)+ ϕ(Hα—Cα—C)(6)+ϕ(C==N—Cα)(5)	

All frequencies are in cm^{-1}.

is the same, the skeletal modes are different. Similarly, the group frequency representation by box distribution or by single frequencies cannot be a true substitute for the density of states. The regions of higher density of states (flat regions) are totally unaccounted for in the box distribution. This approach is also limited when the backbone and side-chain modes are heavily mixed. This is very true in the case of PMet for modes below 1200 cm^{-1}. Thus, the Tarasov two parameter fit is a mere "fit." For PMet, the density of states are shown in Figures 3(b), 4(b), and 5(b). The contributions of purely skeletal, purely side chain, and a mixture of these two to the heat capacities are shown in Figure 6(A), (B), and (C), respectively, in the temperature range of 220–390 K. Total heat capacity is shown in Figure 8(D), and the solid line represents the experimental data of

Table III. Dispersive Modes

Cal.	Obs.	Assignments {% P.E.D. at δ = O)	Cal.	Obs.	Assignments {% P.E.D. at $\delta = 5\pi/9$}
1273	1288	ν(C==Nu0N)(26)+ν(Cα—C)(19)+ν(C==O)(9)+ ϕ(H—N—Cα)(8)+ϕ(Hα—Cα—C)(7)+ϕ(Hα—Cα—Cβ)(7)+ ϕ(O==C==N)(6)+ϕ(C==N—H)(5) {Amide III}	1292	1288	ν(C==NN)(23)+ν(Cα—C)(19)+ν(Cα—N)(9)+ ϕ(Hα—Cα—Cβ)(7)+ν(C==O)(7)+ϕ(Hα—Cα—C)(6)+ ϕ((H—N—Cα)(6)+ϕ(O==C==N)(5) {Amide III}
1084	1073	ν(Cα—Cβ)(24)+CβH$_2$ wag(19)+ν(Cα—C)(15)+ ν(Cα—N)(15)+ϕ(N—Cα—Cβ)(6)	1075	1062	ν(Cα—N)(21)+CβH$_2$ wag(15)+ν(Cα—Cβ)(10)+ ν(Cα—C)(8)+ϕ(N—Cα—Cβ)(7)+ν(C==O)(5)+ϕ(C==N—Cα)(5)
828	838	CγH$_2$ rock(57)+ω(C==O)(6)	821	811	ω(C==O)(18)+CγH$_2$ rock(39)+ω(N—H)(7)
764	766	ω(C==O)(48)+ω(N—H)(26)	778	766	ω(C==O)(31)+ω(N—H)(17)+ν(Cα—Cβ)(9)+CγH$_2$ rock(6)
670	656	ω(N—H)(20)+ω(C==O)(13)+ϕ(N—Cα—C)(12)+ τ(N—Cα)(6) {Amide V + VI}	649	656*	ϕ(O==C==N)(16)+ω(N—H)(13)+ω(C==O)(13)+ τ(N—Cα)(6)+ν(Cα—N)(6)+ϕ(Cα—Cβ—Cγ)(6) {Amide V + VI}
609	618	ω(N—H)(25)+τ(C==N)(14)+ν(Cα—N)(8)+ τ(N—Cα)(8)+ϕ(Cα—CβCγ)(7)+ϕ(O==C==N)(6) {Amide V}	622	630	ω(N—H)(36)+τ(C==N)(13)+ω(C==O)(11)+ τ(N—Cα)(7)+ϕ(O==C==N)(5) {Amide V}
543	548*	ϕ(Cα—C==N)(17)+ϕ(Cα—C==O)(16)+ϕ(N—Cα—Cβ)(13)+ ϕ(Cα—Cβ—Cγ)(8)+ϕ(N—Cα—Hα)(6)+ϕ(N—Cα—C)(5) {Amide IV}	498	496	τ(Sδ—Cε)(40)+ϕ(Cβ—Cγ—Sδ)(12)+ ϕ(Cα—Cβ—Cγ)(7)
478	479	τ(Sδ—Cε)(67)+ϕ(Cβ—Cγ—Sδ)(7)	466	473	τ(Sδ—Cε)(25)+ϕ(N—Cα—Cβ)(9)+ϕ(Cα—C==O)(8)+ ϕ(N—Cα—Hα)(7)+ν(Cα—N)(6)+ϕ(Cα—C==N)(6)+ϕ(Hα—Cα—Cβ)(5)
386	377	ϕ(Cβ—Cγ—Sδ)(35)+τ(Sδ—Cε)(28)	402	420	τ(Sδ—Cε)(32)+ϕ(Cβ—Cγ—Sδ)(17)+ ϕ(Cα—Cβ—Cγ)(11)+ν(Cα—C)(7)
305	306	ϕ(Cγ—Sδ—Cε)(19)+ϕ(O==C==N)(14)+ϕ(C==N—Cα)(13)+ ϕ(C—Cα—Cβ)(12)	319	321	ϕ(Cα—C=O)(13)+ϕ(C==N—Cα)(13)+ ϕ(Cγ—Sδ—Cε)(11)+ ϕ(N—Cα—C)(10)+ϕ(C—Cα—Cβ)(8)+ϕ(O==C==N)(8)
257	257	ϕ(N—Cα—C)(15)+τ(N—Cα)+τ(Cα—C)(12)+ ϕ(C—Cα—Cβ)(9)+ϕ(Cα—C==O)(7)+ ϕ(Cα—C==N)(6)+τ(C==N)(6) {Amide VII}	268	269	ϕ(Cγ—Sδ—Cε)(29)+ϕ(N—Cα—Cβ)(27)+ϕ(C—Cα—Cβ)(6)+ ϕ(Cα—C==N)(5)+τ(Cγ—Sδ)(5)
227	233	ϕ(Cγ—Sδ—Cε)(26)+ϕ(C—Cα—Cβ)(14)+ϕ(N—Cα—Cβ)(14)+ τ(Cα—C)(10)+ϕ(C==N—Cα)(5)	200	200	τ(Cα—C)(17)+ϕ(Cγ—Sδ—Cε)(16)+τ(N—Cα)(13)+ ϕ(C==N—Cα)(10)+ϕ(O==C==N)(7)+ϕ(Cα—C==N)(6)+ τ(Cα—Cβ)(6) {Amide VII}
175	190	ϕ(Cγ—Sδ—Cε)(26)+τ(Cγ—Sδ)(17)+ϕ(C—Cα—Cβ)(10)+ τ(Cα—Cβ)(9)+ϕ(O==C==N)(7)	163	169	ϕ(Cγ—Sδ—Cε)(21)+τ(Cγ—Sδ)(17)+τ(N—Cα)(10)+ ϕ(C—Cα—Cβ)(8)+ϕ(Cα—Cβ—Cγ)(5)
114	—	ϕ(Cα—Cβ—Cγ)(23)+τ(Cα—C)(10)+ϕ(C—Cα—Cβ)(9)+ ϕ(Cβ—Cγ—Sδ)(9)+τ(N—Cα)(8)+τ(Cγ—Sδ)(7)	124	—	τ(Cγ—Sδ)(20)+ϕ(Cα—Cβ—Cγ)(16)+ϕ(C—Cα—Cβ)(9)+ τ(Cα—C)(7)+ϕ(Cβ—Cγ—Sδ)(7)
94	—	τ(Cγ—Sδ)(24)+ϕ(N—Cα—Cβ)(10)+ϕ(Cβ—Cγ—Sδ)(9)+ τ(Cα—Cβ)(9)+ϕ(Cγ—Sδ—Cε)(8)+ϕ(C==N—Cα)(7)+ ϕ(Cα—C==N)(6)	111	—	ϕ(N—Cα—C)(13)+ϕ(C—Cα—Cβ)(10)+τ(Cα—C)(9)+ ϕ(N—Cα—Cβ)(7)+ϕ(C==N—Cα)(6)+ϕ(Cα—Cβ—Cγ)(6)+ ϕ(Cγ—Sδ—Cε)(5)

All the frequencies are in cm^{-1}.
* Indicates backbone modes.

Table IV. Comparision of Amide Modes of α-Helical Polypeptides

	Poly(L-Leucine)		Poly(L-Alanine)		Poly-(L-methionine)	
	$\delta = 0.0$	$\delta = 5\pi/9$	$\delta = 0.0$	$\delta = 5\pi/9$	$\delta = 0.0$	$\delta = 5\pi/9$
Amide A	3313	3313	3293	3293	3296	3296
Amide I	1657	1657	1659	1659	1656	1656
Amide II	1546	1518	1515	1540	1546	1546
Amide III	1299	1318	1270	1274	1288	1288
Amide IV	587	633	525	440	656	656
Amide V	587	617	595	610	618	630
Amide VI	656	633	685	656	656	656
Amide VII	216	—	238	190	257	200

All frequencies are given in cm^{-1}.

Roles et al.[7] With the Tarasov approach, fit to the experimental data is approached in the narrow temperature range of 220 to 250 K. However, a much wider and better fit is obtained with the density of states obtained from the dispersion curves. There are fewer deviations throughout. Overall calculations are in much better agreement with the experimental measurements. At the low temperature end the calculated curve falls slightly above the experimental points, which is mainly due to the neglect of low-frequency lattice modes. In the higher region the experimental heat capacity is found to have slightly higher values than those calculated. It could be for more than one reasons. Our calculations support the observation made by Roles et al.[7] According to them, this discrepancy may be due to the gradual glass transition undergone by the sample. X-ray diffraction studies also reveal a low degree of crystallinity. The contribution from anharmonic effects and lattice modes, which may fall in the same region as torsional modes, are also bound to make an

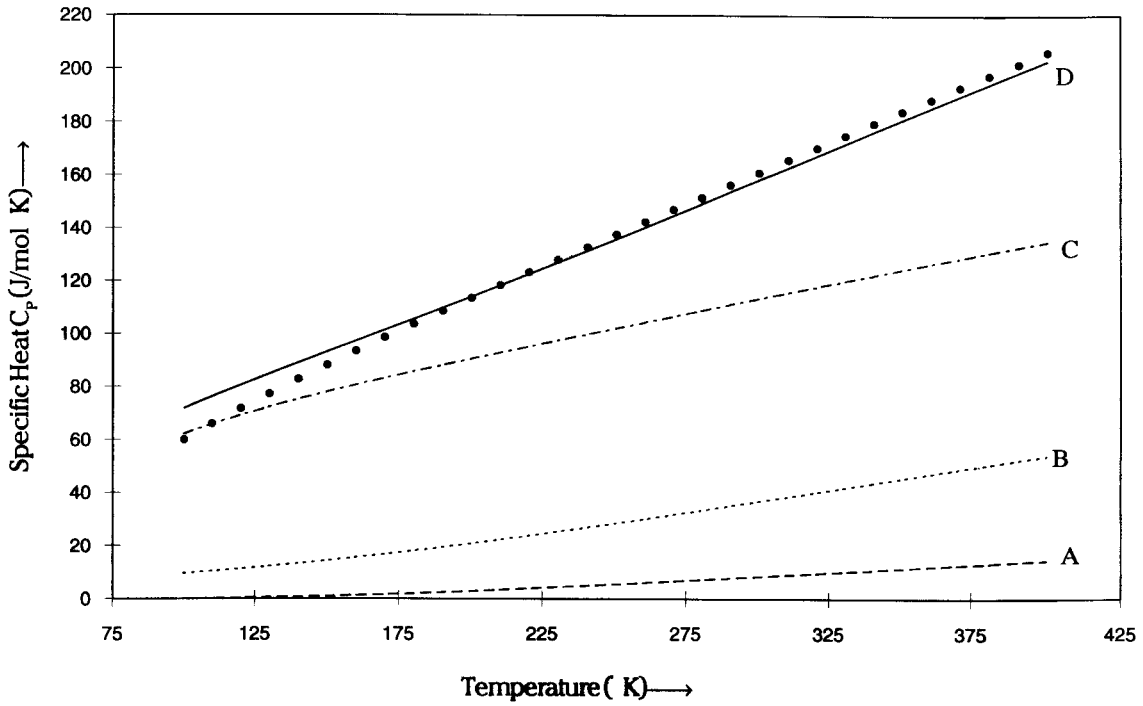

Figure 6. Variation of heat capacity Cp of poly(L-methionine) with temperature. (A) (---) Contribution of backbone modes, (B) (· · · · · ·) Contribution of side chain modes. (C) (· – · – · –) Contribution of mix modes, (D) (——) Total heat capacity and (· · ·) experimental data.

appreciable difference to the heat capacity. The anharmonic effects mainly arise in the torsional potentials. At the moment, the calculation for dispersion curves for a unit cell are extremely difficult because even if we assume a minimum of two chains in unit cell then there would be 170 atoms leading to a matrix of 510 $\times$ 510. It would bring in an enormous number of interactions and make the problem almost intractable. Thus, in spite of several limitations involved in the calculation of specific heat, the present work does provide a good starting point for further basic studies on thermodynamical behavior of polypeptides and proteins that go into well-defined conformations.

Financial assistance to V.D.G. from the Council for Scientific & Industrial Research, New Delhi, under the Emeritus Scientist Scheme and to P.T. from the Department of Science & Technology, New Delhi, under the Young Scientist Scheme is gratefully acknowledged.

REFERENCES AND NOTES

1. P. Tandon, V. D. Gupta, O. Prasad, S. Rastogi, and S. B. Katti, *J. Polym. Sci. B: Polym. Phys.,* **34,** 1213 (1996).
2. G. D. Fasman, in *Poly-α Amino Acids: Protein Models for Conformational Studies,* G. D. Fasman, Ed., Marcel Dekker, Inc., New York, 1967, p. 499.
3. S. M. Bloom, G. D. Fasman, C. De Loze, and E. R. Blout, *J. Am. Chem. Soc.,* **84,** 458 (1962).
4. B. Wunderlich and H. S. Bu, *Thermochim. Acta,* **119,** 225 (1987).
5. H. S. Bu, W. Aycock, Z. D. Cheng Stephen, and B. Wunderlich, *Polymer,* **29,** 1486 (1988).
6. K. A. Roles and B. Wunderlich, *Biopolymers,* **31,** 477 (1991).
7. K. A. Roles, A. Xenopoulos, and B. Wunderlich, *Biopolymers,* **33,** 753 (1993).
8. D. Gani, P. J. Hendra, W. F. Maddams, C. Passingham, I. A. M. Royald, H. A. Willis, and V. Zichy, *Analyst,* **115,** 1313 (1990).
9. M. V. Krishnan and V. D. Gupta, *Chem. Phys. Lett.,* **6,** 231 (1970).
10. M. V. Krishnan and V. D. Gupta, *Chem. Phys. Lett.,* **7,** 285 (1970).
11. V. D. Gupta, S. Trevino, and H. Boutin, *J. Chem. Phys.,* **48,** 3008 (1968).
12. R. D. Singh and V. D. Gupta, *Spectrochim. Acta,* **27A,** 385 (1971).
13. L. Burman, P. Tandon, V. D. Gupta, S. Rastogi, S. Srivastava, and G. P. Gupta, *J. Macromol. Sci.-Phys.,* **B34,** 479 (1995).
14. A. Gupta, P. Tandon, V. D. Gupta, S. Rastogi, and G. P. Gupta, *J. Macromol. Sci.-Phys.,* **B34,** 501 (1995).
15. A. M. Dwivedi and V. D. Gupta, *Chem. Phys. Lett.,* **16,** 909 (1972).
16. V. D. Gupta, R. D. Singh, and A. M. Dwivedi, *Biopolymers,* **12,** 1377 (1973).
17. R. B. Srivastava and V. D. Gupta, *Biopolymers,* **13,** 1965 (1974).
18. O. Prasad, P. Tandon, V. D. Gupta, and S. Rastogi, *Polymer,* **36,** 2739 (1995).
19. E. B. Wilson, J. C. Decuis, and P. C. Cross, *Molecular Vibrations: The Theory of Infrared and Raman Vibrational Spectra,* Dover Publications, New York, 1980.
20. P. W. Higgs, *Proc. R. Soc. (Lond.),* **A220,** 472 (1953).
21. R. Pan, M. Verma–Nair, and B. Wunderlich, *J. Therm. Anal.,* **35,** 955 (1989).
22. S. Krimm and J. Bandekar, *Adv. Protein. Chem.,* **38,** 181 (1986).
23. M. J. Hanon, F. J. Boerio, and J. L. Koenig, *J. Chem. Phys.,* **50,** 2829 (1969).
24. D. I. Bower and W. F. Maddams, *The Vibrational Spectroscopy of Polymers,* Cambridge University Press, Cambridge, 1989, p. 154.